Model for density-functional thermodynamic perturbation analysis of Lennard-Jones solids

Agathagelos Kyrlidis and Robert A. Brown

Department of Chemical Engineering, Massachusetts Institute of Technology, Cambridge, Massachusetts 02139
(Received 2 July 1992)

Thermodynamic perturbation theory and density-functional approximations are systematically combined to produce a model of Lennard-Jones solids and solid-liquid coexistence. The perturbation theory is based on expanding the free energy about that of the fcc hard-sphere solid, which is described by an accurate nonperturbative density-functional theory. Approximations made throughout the development are systematically checked against results of Monte Carlo simulations. The Gaussian approximation used for describing the solid density is shown to be a good approximation for the stable solid; however, anisotropies in the structure that are not captured by the Gaussian approximation become pronounced at densities corresponding to metastable solids. The free energies of both the solid and the liquid Lennard-Jones phases and the phase diagram predicted by the density-functional thermodynamic perturbation model are in good agreement with Monte Carlo simulations for temperatures in the range $0.75 \leq kT/\varepsilon \leq 100$.

I. INTRODUCTION

Developments in density-functional theory (DFT) have made possible the unified modeling of inhomogeneous solids and liquids [1–3]. The centerpiece of the various DFT approximations is the free-energy functional $F[\rho(\mathbf{r})]$, which is generated using information about the uniform liquid that is readily available from liquid-state theory and atomistic simulations. Several recent density-functional approximations make assumptions that link the thermodynamic and structural properties of the inhomogeneous solid or liquid system to those of the well-characterized liquid [4–8]. Here the microscopic density variations in the inhomogeneous system are approximated by convenient numerical or functional representations and the total system free energy is then minimized to yield the approximate optimal structure and free energy for the inhomogeneous system.

The great flexibility of DFT is seen in the large variety of problems that have been studied; these range from structured simple liquids (liquids confined in narrow slit pores [9,10], wetting and drying transitions [11,12]) to homogeneous and inhomogeneous solids (solid-liquid coexistence [4–8], melt-solid interface [13]). A recent review of some of the applications of DFT to ordering problems is given by Singh [3]. Models for structured simple liquids are not very sensitive to the nature of the approximations made for the free-energy functional [9] and simple weighted density approximations yield results in reasonable agreement with the predictions of atomistic simulations [9,11]. Unfortunately, the study of solids is more complicated, because the solid has more structure than confined liquids, and its density varies in every spatial dimension. The solid calculations are simplified by the periodicity of the crystalline lattice, but more complex free-energy functionals are required to accurately capture the thermodynamics of the solid state [5].

Most research into density-functional theories for solids has focused on the description of the hard-sphere (HS) solid, because accurate liquid-state information is available for this system in analytical form. Recently developed nonperturbative functionals, based on a combination of *thermodynamic* and *structural* mappings of the inhomogeneous system to the uniform liquid, have predicted accurately the free energy of the hard-sphere solid. For example, the nonperturbative DFT's in [7,8] predict the conditions of solid-liquid coexistence within less than 1% of the results of atomistic simulations. However, the prediction of solid structure is not so good; for example, most DFT approximations overpredict the degree of structured order of the hard-sphere solid at a given density [14]. The reasons behind this inaccuracy have not been determined.

The extension of nonperturbative DFT approximations to more complicated potentials has encountered several difficulties. Laird and Kroll [15] studied the soft-sphere system and found that both the modified weighted density [6] and the generalized effective liquid [7] approximations fail when applied directly to the solid phase. De Kuijper et al. [16] also attempted the direct application of DFT to the Lennard-Jones (LJ) system, but obtained poor results at low temperatures. In a recent paper [17] we argued that solids described by interatomic potentials that include an attractive contribution cannot be stabilized by the current DFT approximations at low temperatures. We believe that an accurate combination of density-functional approximations and thermodynamic-pertur- bation analysis is necessary for describing such systems; we refer to such models as DF-TP theories.

Several DF and DF-TP studies of the LJ system have appeared in the last decade [4,13,16,18,19]. However, most of the DF-TP formulations were not based on a thermodynamic perturbation framework that is accurate for high-density liquids and solids. Moreover, little attention has been given to how well the structure of the reference state is represented for the perturbation

analysis. Simultaneously, thermodynamic perturbation theories have appeared [20,21] for solids and high-density liquids based on structural information provided by atomistic simulations. These studies are very important as tests of the accuracy of the approximations involved in the thermodynamic perturbation analysis. Such tests are emphasized here.

In this paper we present a model for the LJ system based on the coupling of an accurate DFT approximation for the hard-sphere system with an accurate thermodynamic perturbation framework. The principles of the DFT approximations are briefly reviewed in Sec. II. Monte Carlo simulations of hard-sphere solids are used to provide information about the accuracy of the structural predictions of the DFT. The thermodynamic perturbation framework is outlined in Sec. III, and its advantages with respect to more traditional approaches are discussed. The approximations made in the DF-TP model of the solid phase are discussed in Sec. IV and predictions are presented for the free energy. Calculations of solid-liquid coexistence for the LJ system are presented in Sec. V.

II. DESCRIPTION OF THE HARD-SPHERE SOLID

A. Free-energy functional

Evans [1] has shown that the excess free energy of an inhomogeneous system is given by the expression

$$\beta F_{ex} = -\int d\mathbf{r} \int d\mathbf{r}' \int_0^1 d\lambda (1-\lambda)\rho(\mathbf{r})\rho(\mathbf{r}')$$
$$\times c^{(2)}(\mathbf{r},\mathbf{r}';[\lambda\rho]) , \qquad (1)$$

where $\beta \equiv 1/kT$ and $c^{(2)}(\mathbf{r},\mathbf{r}')$ is the unknown direct correlation function of the inhomogeneous system.

This excess free energy is approximated by a *thermodynamic* mapping [4,5] that transforms the local excess free energy per particle of the inhomogeneous system to the excess free energy per particle f_0 of a uniform system. There are two ways that this mapping can be constructed. It may be approximated *locally* using a spatially varying *weighted* density $\bar{\rho}(\mathbf{r})$ [4,5]

$$F_{ex} = \int d\mathbf{r}\rho(\mathbf{r})f_0(\bar{\rho}(\mathbf{r};[\rho])) , \qquad (2)$$

or *globally* using a spatially invariant weighted density $\hat{\rho}$ [6,7]

$$F_{ex} = Nf_0(\hat{\rho}[\rho]) . \qquad (3)$$

The necessary closure approximations for the evaluation of the weighted densities $\bar{\rho}(\mathbf{r})$ or $\hat{\rho}$ are given by a second approximation, the *structural* mapping [7], which in the local generalized effective liquid approximation (LGELA) [8] requires that

$$\int d\mathbf{r} \int d\mathbf{r}'\rho(\mathbf{r})\rho(\mathbf{r}')c^{(2)}(\mathbf{r},\mathbf{r}';[\rho])$$
$$= \int d\mathbf{r} \int d\mathbf{r}'\rho(\mathbf{r})\rho(\mathbf{r}')c_0^{(2)}[|\mathbf{r}-\mathbf{r}'|;\bar{\rho}(\mathbf{r})] , \qquad (4)$$

where $c_0^{(2)}(|\mathbf{r}-\mathbf{r}'|)$ is the direct correlation function of the uniform liquid, and in the generalized effective liquid approximation (GELA) [7]

$$\int d\mathbf{r} \int d\mathbf{r}'\rho(\mathbf{r})\rho(\mathbf{r}')c^{(2)}(\mathbf{r},\mathbf{r}';[\rho])$$
$$= \int d\mathbf{r} \int d\mathbf{r}'\rho(\mathbf{r})\rho(\mathbf{r}')c_0^{(2)}(|\mathbf{r}-\mathbf{r}'|;\hat{\rho}) . \qquad (5)$$

The total free energy of the inhomogeneous system in the absence of an external field is

$$\beta F = \int d\mathbf{r}\rho(\mathbf{r})\{\ln\Lambda^3\rho(\mathbf{r})-1\} + \beta F_{ex}[\rho] , \qquad (6)$$

where Λ is the thermal wavelength. For the hard-sphere fluid, the uniform liquid excess free energy f_0 is computed from the Carnahan-Starling (CS) equation of state, and the uniform liquid direct correlation function $c_0^{(2)}(r)$ is calculated from the Percus-Yevick (PY) approximation [22]; see [1] for more details on the theoretical basis of DFT.

B. Solid density approximation

The free-energy functional $F[\rho(\mathbf{r})]$ defined by Eq. (6) is valid for any inhomogeneous solid or liquid. An additional approximation for the density profile of the inhomogeneous system is required to reduce the search for $\rho(\mathbf{r})$ to a finite-dimensional problem. This approximation introduces a set of unknown parameters with respect to which the total free energy is minimized. Ideally, the parametrization of the density is based on numerical functional approximations that are flexible and have accuracy that can be monitored and controlled. Such approximations have been used extensively in the study of one-dimensional problems, such as the structure of fluids confined by solid surfaces [9]. Additional constraints also are required that guarantee the positivity of the density; these constraints are either explicitly introduced in the free-energy minimization or satisfied directly through a functional transformation of the density [9,23].

In solids the density variations are three dimensional and extend periodically throughout the bulk. The DFT formulation could be based on the discretization of a three-dimensional spatially periodic supercell, the use of a numerical functional approximation of the density and a subsequent free-energy minimization without any specification of the lattice symmetries. However, there are practical and computational problems with such an approach, that have eliminated it from consideration in the description of solids. In the development of density parametrizations for solids the issue of spontaneous symmetry breaking during the liquid-solid phase transition has been neglected, and the crystalline structure has been *selected a priori*. The first DFT studies of solids [24,25] used a density-wave representation of the crystalline structure in which the solid density was approximated as

$$\rho(\mathbf{r}) = \rho_l + (\rho_s - \rho_l)\hat{\rho}_0 + \sum_{\mathbf{k}\,(\neq 0)} \hat{\rho}_k \exp(i\mathbf{k}\cdot\mathbf{r}) , \qquad (7)$$

where $\{\mathbf{k}\}$ is the set of reciprocal lattice vectors (RLV's) of the crystalline lattice, and $\{\hat{\rho}_k\}$ is the set of Fourier coefficients that are used as variational parameters in the free-energy minimization.

The density-wave parametrization (7) represents a dramatic decrease in the number of parameters in the

solid density approximation, and makes no direct assumptions about the isotropy of the solid. However, keeping a small number of RLV's leads to aphysical regions of negative density, as pointed out by Baus and Colot [26]. For a structured solid close to the coexistence density, more than 50 of these coefficients are required for the series (7) to converge and for the density to remain positive throughout the unit cell. Harrowell, Oxtoby, and Haymet [23] demonstrated that a transformed version of Eq. (7) was well behaved, even when a small number of RLV's was used in their DFT. To avoid the problems of the density-wave representation Tarazona [4] used a Gaussian representation of the solid density in physical space as

$$\rho(\mathbf{r}) = \left[\frac{\alpha}{\pi}\right]^{3/2} \sum_{\mathbf{R}} \exp[-\alpha(\mathbf{r} - \mathbf{R})^2] \ , \tag{8}$$

where $\{\mathbf{R}\}$ are the real-space lattice vectors. This representation of the solid density is always positive. Moreover, it introduces only *one* variational parameter, the inverse width of the Gaussian α, which is a measure of the localization in the crystal. The application of the Gaussian parametrization (8), with the GELA and LGELA DFT approximations described previously, gives very accurate predictions of the free energies of hard-sphere solids, as is reported in Refs. [7,8].

Colot and Baus [27] tested the accuracy of the Gaussian approximation by introducing non-Gaussian behavior near the "tail" of the density peak and found that these corrections did not shift the minimum of the free energy from the results of the Gaussian approximation. Laird, McCoy, and Haymet [28] compared density profiles predicted by their DFT for hard spheres for Gaussian and density-wave representations of the solid phase, and found that the density-wave representation resulted in significant anisotropies in the density that were excluded by the Gaussian representation.

Comparisons of the structural predictions of DFT approximations to atomistic simulation results have been for the Lindemann factor of the hard-sphere system at coexistence, and the stable crystalline lattice symmetry and lattice parameter. The Lindemann factor L is defined as the ratio of the mean amplitude of the thermal vibrations in the crystal to the nearest-neighbor interatomic separation [24,26]:

$$L \equiv \langle |\mathbf{r} - \mathbf{R}|^2 \rangle^{1/2} / r_{\mathrm{NN}} \ , \tag{9}$$

where $\mathbf{R}$ is the position vector for the perfect crystalline lattice, and r_{NN} is the nearest-neighbor separation. The Lindemann factor is linked to the localization parameter α of the Gaussian parametrization through a quasiharmonic crystalline representation. For the fcc crystalline lattice studied here for the hard-sphere system L is [26]

$$L = \left[\frac{3}{\alpha a^2}\right]^{1/2} \ , \tag{10}$$

where a is the lattice constant. Simulations have yielded various values for the Lindemann factor at the coexistence density; for liquid argon $L = 0.1 - 0.14$ [24] and

for the hard-sphere system $L = 0.126$ [29]. Little data has been reported for the variation of L with density for a hard-sphere system.

Two issues involving the structural representation are particularly important for constructing accurate DFT's. First, how good is the Gaussian approximation for the range of densities where it is typically used? And specifically, are there any anisotropies in the solid density that are excluded by the Gaussian approximation? Second, how does the structure of the hard-sphere solid, as measured by the localization parameter α, vary with density? We performed a series of Monte Carlo (MC) simulations for hard-sphere solids to answer these questions.

The simulations were based on 500 and 864 particles arranged in a periodic cubic supercell. Particles were moved individually according to the Metropolis algorithm [30]; a Monte Carlo sweep refers to trial moves for all particles. Starting with a perfect fcc configuration at the coexistence density, one long simulation (250 000 sweeps) was used to generate a starting configuration for the subsequent simulations. Approximately 10^5 sweeps were discarded each time to avoid any influences of the initial positions. The typical simulation at each density was comprised of 250 000 sweeps.

The simulations were used to measure the three-dimensional density profile within the unit cell of the fcc lattice. For this purpose the center of mass of the simulation cell was fixed to the perfect crystal position. Each simulation cell consisted of $5^3 = 125$ and $6^3 = 216$ unit cells for the 500 and 864 particle systems, so each sweep through the particles corresponded to 125 and 216 unit-cell configurations, respectively. Approximately $(2-3) \times 10^7$ unit-cell configurations were used for constructing averages. The unit cell was split into 40 bins in each spatial dimension and the value of the density at the center of each bin (x_b, y_b, z_b) was computed as

$$\rho(x_b, y_b, z_b) = K^{-1} \sum_{i=1}^{N} \sum_{j=1}^{M} \delta(\hat{x}_i - x_b) \delta(\hat{y}_i - y_b)$$
$$\times \delta(\hat{z}_i - z_b) \ , \tag{11}$$

where N is the number of particles,

$$\hat{x}_i = x_i - a\,\mathrm{int}(x_i/a) \ , \tag{12}$$

is the mapping of particle positions to the single unit cell, and int corresponds to the integer portion of the argument,

$$\delta(\hat{x}_i - x_b) = \begin{cases} 1, & x_b - \Delta x/2 \leq \hat{x}_i \leq x_b + \Delta x/2 \\ 0, & \text{otherwise} \end{cases} \tag{13}$$

and $K \equiv M(l/a)^3 \Delta x \Delta y \Delta z$, where M is the number of particle sweeps in the simulation, l is the length of the simulation cell, a is the lattice constant and $\Delta x = \Delta y = \Delta z = a/40$ are the dimensions of the bins.

The coefficients $\{\hat{\rho}_{\mathbf{k}}\}$ in the Fourier expansion of the density are computed directly from

$$\hat{\rho}_{\mathbf{k}} \equiv \frac{1}{V} \int d\mathbf{r}\, \rho(\mathbf{r}) \exp(-i\mathbf{k}\cdot\mathbf{r}) \ . \tag{14}$$
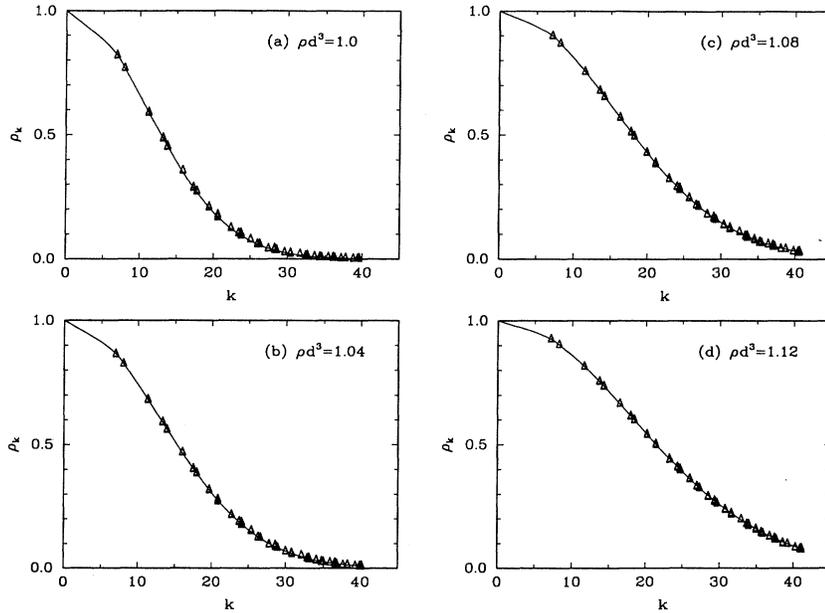
FIG. 1. Comparison of Fourier coefficients $\rho_k \equiv \hat{\rho}_{|k|}/\rho$ predicted by MC simulations ($\triangle$) and best fit of the Gaussian approximation (———) for the hard-sphere solid, at (a) $\rho d^3 = 1.0$, (b) $\rho d^3 = 1.04$, (c) $\rho d^3 = 1.08$, and (d) $\rho d^3 = 1.12$.

The variation of $\rho_k \equiv \hat{\rho}_k/\rho$ with k, where ρ is the average solid density, is shown in Fig. 1 for hard-sphere solids with $1 \leq \rho d^3 \leq 1.12$ as predicted from the MC simulations. This variation strongly resembles the Gaussian prescription for $\rho_k = \exp(-k^2/4\alpha)$, particularly for densities satisfying $\rho d^3 > 1$.

The values of α that led to the best approximation to the MC results are plotted in Fig. 2 as a function of the solid density. These results are compared to the values of α that minimize the solid free energy within the GELA-DFT formulation. It is clear that the GELA-DFT overpredicts the structure of the HS solid throughout the density range $0.95 \leq \rho d^3 \leq 1.12$. At the coexistence density of $\rho d^3 = 1.041$ predicted by GELA, the Lindemann factor, as found from these Monte Carlo simulations and Eq. (10), is $L \simeq 0.122$; the GELA prediction is $L = 0.1$, as reported in [7]. The difference between this prediction of the Lindemann factor and the value reported by Hoover and Ree [29] derives from differences in the simulation methods. Hoover and Ree used the "single occupancy cell" method to localize the solid, whereas in this study the center of mass of the simulation supercell was kept fixed in order to obtain meaningful density profiles in the unit cell. The effect of this constraint depends on the size of the simulation cell and it can be minimized by increasing the number of particles in the simulation; for $N = 2916$ particles, the Lindemann factor is $L \simeq 0.125$, in better agreement with Hoover and Ree.
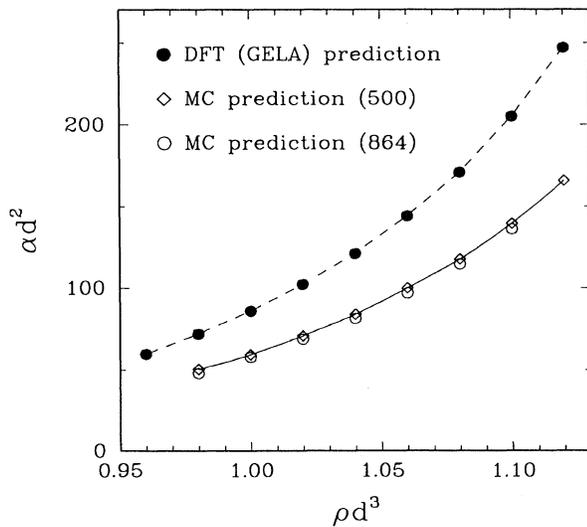
The computation of the three-dimensional density profile in the unit cell from the Monte Carlo simulations allows the study of possible anisotropies of the solid density. Contours of the z-averaged density $\rho(x,y) = (1/a)\int\rho(r)dz$ computed from the MC simulations are presented in Figs. 3 and 4, and are compared to the Gaussian predictions with the corresponding values of α; the values of the density used are $\rho d^3 = 0.96$, which is well within the metastable solid region, and $\rho d^3 = 1.1$, respectively. The structure of the peak centered at (0,0,0) is seen more clearly in the plots of $4\pi r^2\rho(r)d$ in the three main crystallographic directions [100], [110], and [111], which also are presented in Figs. 3 and 4 for the two values of the density. Some deviations from the Gaussian model are visible in Fig. 3, but these anisotropies become less apparent as the density is increased. The deviations from the Gaussian approximation for $\rho d^3 = 0.96$ are similar to those predicted by Laird, McCoy, and Haymet [28]

FIG. 2. Comparison of the localization αd^2 predicted from MC simulations with 500 and 864 particles of the hard-sphere solid, and the predictions of the GELA density-functional theory for $0.96 \leq \rho d^3 \leq 1.12$.
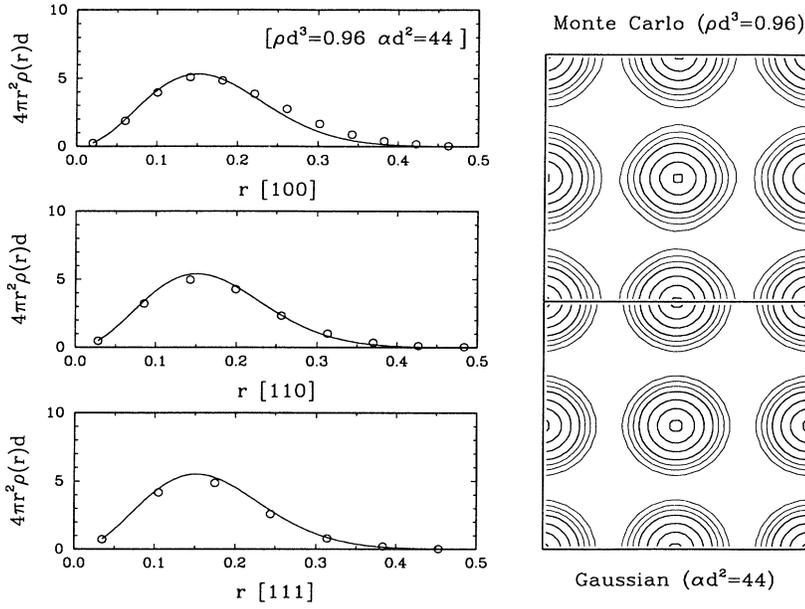
FIG. 3. Density profiles $4\pi r^2 \rho(\mathbf{r})d$ plotted along the [100], [110], and [111] directions in the unit cell for the Gaussian peak centered at (0,0,0), for a solid with $\rho d^3 = 0.96$; r is scaled by the hard-sphere diameter d. The solid curve corresponds to the Gaussian approximation with $\alpha d^2 = 44$, and ($\circ$) to the MC results. Contours of the z-averaged densities in the unit cell (0.1, 0.25, 0.5, 1.0, 2.5, 5.0, and 8.0) predicted from the MC simulations and the Gaussian approximation also are compared.

and discussed by Oxtoby [2], but the differences appear at a much smaller density. The density is greater than the Gaussian prediction along directions in the crystal where the interatomic distances are largest. The effect of this anisotropy becomes less important at higher solid densities and the use of the Gaussian approximations in DFT models for the solid seems justified.

A possible explanation for the failure of most DFT approximations to predict the correct degree of localization in the solid is that the structural mapping does not approximate correctly the strength of pair correlations in the solid. This approximation creates a more structured solid to counteract the ideal-gas contribution to the total free energy, which acts as a balancing term in the minimization of the free energy with respect to the localization parameter α. For the purposes of this work, the GELA and LGELA approximations of the hard-sphere free energy are accurate enough to warrant the use of the hard-sphere solid as a reference state for the thermodynamic perturbation study of solids described by the LJ interatomic potential.

III. THERMODYNAMIC PERTURBATION THEORY: THE LJ LIQUID

Thermodynamic perturbation analyses have been used extensively in the last few decades [22,31,32] in studies of
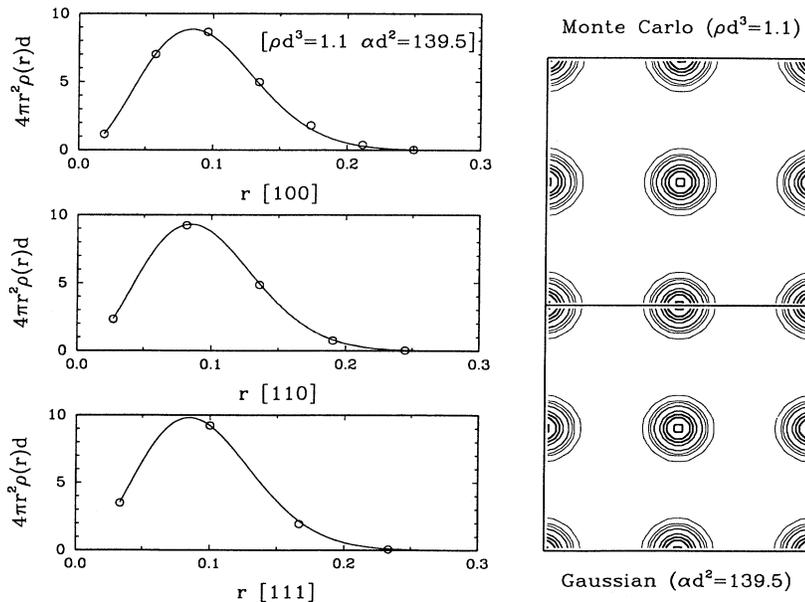
FIG. 4. Density profiles $4\pi r^2 \rho(\mathbf{r})d$ plotted along the [100], [110], and [111] directions in the unit cell for the Gaussian peak centered at (0,0,0), for a solid with $\rho d^3 = 1.1$; r is scaled by the hard-sphere diameter d. The solid curve corresponds to the Gaussian approximation with $\alpha d^2 = 139.5$, and ($\circ$) to the MC results. Contours of the z-averaged densities in the unit cell (0.1, 0.5, 1.0, 2.0, 6.0, 10.0, 15.0, and 25.0) predicted from the MC simulations and the Gaussian approximation also are compared.

the properties of homogeneous liquids described by simple interatomic potentials. The LJ system described by the pair potential

$$U_{LJ}(r) = 4\varepsilon\left[\left[\frac{\sigma}{r}\right]^{12} - \left[\frac{\sigma}{r}\right]^6\right]$$

has been studied extensively, where ε and σ are the energy and length scales of this interatomic potential. The centerpiece of the thermodynamic perturbation method is the decomposition [22] of the pairwise potential to

$$U_\lambda(r) = U_{\lambda_0}(r) + (\lambda - \lambda_0)U_1(r) , \tag{15}$$

where U_{λ_0} is the reference state potential, λ is a coupling parameter, and U_1 is the contribution defined so that if $\lambda = \lambda_1$, U_{λ_1} is the complete interatomic potential. In most studies the decomposition of the LJ potential has been written with $\lambda_0 = 0$ and $\lambda_1 = 1$ [22], so that Eq. (15) reduces to

$$U_{LJ}(r) = U_0(r) + U_1(r) . \tag{16}$$

Zwanzig [32] showed that it is possible to expand the free energy of a system whose potential has been decomposed according to Eq. (16), as an expansion in β about the reference potential U_0. The free energy becomes

$$F = F_0 + \frac{\rho^2 V}{2}\int d\mathbf{r}\, U_1(r)g_0(r) + \cdots , \tag{17}$$

where F_0 is the free energy of the reference state system, and $g_0(r)$ is the pair distribution function of the reference state and the ellipsis signifies higher-order terms.

Because the reference state is not necessarily better known than the full LJ system, it is important to link its properties to the hard-sphere system:

$$U_{hs}(r) = \begin{cases} \infty , & \text{for } r < d \\ 0, & \text{for } r > d , \end{cases}$$

where d is the hard-sphere diameter. The hard-sphere liquid is well described by the CS equation of state and PY pair distribution function [22]. The PY approximation is used in this work for consistency with the liquid description used in the DFT instead of the more accurate pair distribution function that was developed by Verlet and Weiss [33]. The solid is accurately modeled by the DFT approximations discussed in the previous section. The mapping to an effective hard-sphere system is accomplished by defining

$$d \equiv d[U_0(r); \rho, T] , \tag{18}$$

where d is the effective hard-sphere diameter.

The blip function $\Delta e(r) \equiv \{\exp[-\beta U_0(r)] - \exp[-\beta U_{HS}(r)]\}$ is used as a measure of the hardness of the reference state [22] and is the link between the reference state free energy F_0 and that of an equivalent hard-sphere system through a functional expansion of F_0 in terms of $\Delta e(r)$:

$$F_0 = F_d - \frac{1}{2}\frac{\rho^2 V}{\beta}\int d\mathbf{r}\, y_d(r)\Delta e(r) + \cdots , \tag{19}$$

where $y_d \equiv g_d(r)\exp[\beta U_{HS}(r)]$ and the subscript d denotes hard-sphere liquid properties. Neglecting higher-order contributions gives $F_0 = F_d$ for an effective diameter of a hard-sphere system that satisfies

$$\int d\mathbf{r}\, y_d(r)\Delta e(r) = 0 . \tag{20}$$

The mapping condition (20) was introduced by Andersen, Weeks, and Chandler [34] and yields an effective hard-sphere diameter that is a function of both density and temperature.

There are three key steps in developing an accurate thermodynamic perturbation framework: a good potential decomposition scheme must be selected; an accurate mapping of the reference state to an effective hard-sphere system must be developed; and the perturbative contribution to the total free energy of the system must be computed efficiently. Each of these issues is considered in turn.

A. Potential decomposition: Effective hard-sphere system

Most previous DF-TP analyses have been based on the Barker-Henderson (BH) potential decomposition [22], according to which

$$U_0(r) \equiv \begin{cases} U_{LJ}(r) , & \text{for } r < \sigma \\ 0 , & \text{for } r > \sigma , \end{cases}$$
$$U_1(r) \equiv \begin{cases} 0, & \text{for } r < \sigma \\ U_{LJ}(r) , & \text{for } r > \sigma . \end{cases} \tag{21}$$

The corresponding prescription for the effective hard-sphere diameter is

$$d = \int_0^\infty dr\{1 - \exp[-\beta U_0(r)]\} . \tag{22}$$

Equation (22) has been widely used and is relatively accurate. Verlet and Weiss [33] have shown that Eq. (22) results from the leading-order term in Eq. (20), if $r^2 y_d(r)$ is expanded in a Taylor series about its value at $r = d$. Equation (20) was used by Weeks, Chandler, and Andersen (WCA) [35] with the potential split into purely repulsive and purely attractive parts

$$U_0(r) \equiv \begin{cases} U_{LJ} + \varepsilon, & \text{for } r < 2^{1/6}\sigma \\ 0, & \text{for } r > 2^{1/6}\sigma , \end{cases}$$
$$U_1(r) \equiv \begin{cases} -\varepsilon, & \text{for } r < 2^{1/6}\sigma \\ U_{LJ}(r), & \text{for } r > 2^{1/6}\sigma . \end{cases} \tag{23}$$

The WCA decomposition converges faster than the BH decomposition, especially for the high-density liquids that are used in the study of solid-liquid coexistence [35]. Both of these decompositions are not useful at high temperatures because the reference potential becomes too soft and the effective hard-sphere system densities become unrealistically high [36].

Kang et al. [37] introduced a density-dependent potential splitting, which maintains the rapid convergence of the WCA decomposition and reduces the effective hard-sphere density by shrinking the range of the reference repulsive potential to the nearest-neighbor distance of an

fcc lattice. This decomposition is

$$U_0(r) \equiv \begin{cases} U_{LJ}(r) - F(r), & \text{for } r < \lambda \\ 0, & \text{for } r > \lambda \ , \end{cases}$$

$$U_1(r) \equiv \begin{cases} F(r), & \text{for } r < \lambda \\ U_{LJ}(r), & \text{for } r > \lambda \ , \end{cases} \qquad (24)$$

where the function $F(r)$ is defined as

$$F(r) \equiv U_{LJ}(\lambda) - U'_{LJ}(\lambda)(\lambda - r) \ ,$$

with $\qquad\qquad\qquad\qquad\qquad\qquad\qquad\qquad (25)$

$$\lambda \equiv \min\{2^{1/6}\sigma, 2^{1/6}/\rho^{1/3}\} \ .$$

We use the definition of λ given in Kim, Ree, and Ree [38] that varies continuously between $2^{1/6}\sigma$ and the density-dependent cutoff. Previous calculations of the

effective hard-sphere diameter performed with the original prescription of Kang *et al.* [37] do not differ significantly [39].

The advantages of the Kang *et al.* [37] decomposition for the study of high-temperature systems are apparent in Fig. 5, where the range of LJ densities that is accessible using a hard-sphere reference state with densities $0.92 \leq \rho d^3 \leq 1.1$ are compared for several decomposition schemes and prescriptions for the effective hard-sphere system. Our goal is to accurately represent LJ solids and liquids with densities in the vicinity of the melting and freezing point. While at low temperatures, the BH decomposition scheme is well behaved, it maps a LJ liquid at the freezing density to a hard-sphere system with an unreasonably high density at very high temperatures. The same inaccuracy is inherent to the WCA decomposition scheme. The advantage of the Kang *et al.* decomposition is that at $kT/\varepsilon = 100$ the range of LJ densities $2.2 \leq \rho \sigma^3 \leq 3.2$ can be spanned from the range of hard-sphere liquid densities $0.92 \leq \rho d^3 \leq 1.1$ Using the BH prescription for the effective hard-sphere diameter for this potential decomposition scheme also yields reasonable results for d; however, neglecting higher-order contributions leads to larger values of the free energy than with effective hard-sphere diameters estimated from the WCA Eq. (20).

B. Pair distribution function

WCA used the approximation [35]

$$g_0(r) = y_d(r)\exp[-\beta U_0(r)] \ , \qquad (26)$$

which is equivalent to

$$g_0(r) = y_d(r)\exp[-\beta U_{hs}(r)] \qquad (27)$$

for the WCA potential decomposition [33]. Equation (27) does not require $y_d(r)$ for $r < d$. However, Eqs. (26) and (27) are not equivalent for the potential decomposition of Eq. (24) at densities $\rho \sigma^3 > 1$. Calculations using both prescriptions for the reference state structure are presented here to study the effect of these approximations on the predicted values for the free energy. The Percus-Yevick approximation $y_d(r) = g_d(r) - c_d(r)$ is used for the hard-sphere system [40]. The technique described by Frisch *et al.* [41] is employed to compute the long-range perturbative contributions to the free energy after making the appropriate adjustments for the Kang *et al.* potential decomposition scheme.

The predictions of this framework for the excess free energies of uniform LJ liquids are shown in Table I for a range of temperatures, and are compared with the exact values from MC simulations, and the predictions of Kang *et al.* [37]. Our approximations are accurate over the entire temperature range $0.75 \leq kT/\varepsilon \leq 100$. These results confirm the accuracy of the TP framework for the description of uniform LJ liquids. Using Eq. (27) improves the predictions at higher densities. This was also observed by Kang *et al.* [37]. Equations (26) and (27) are
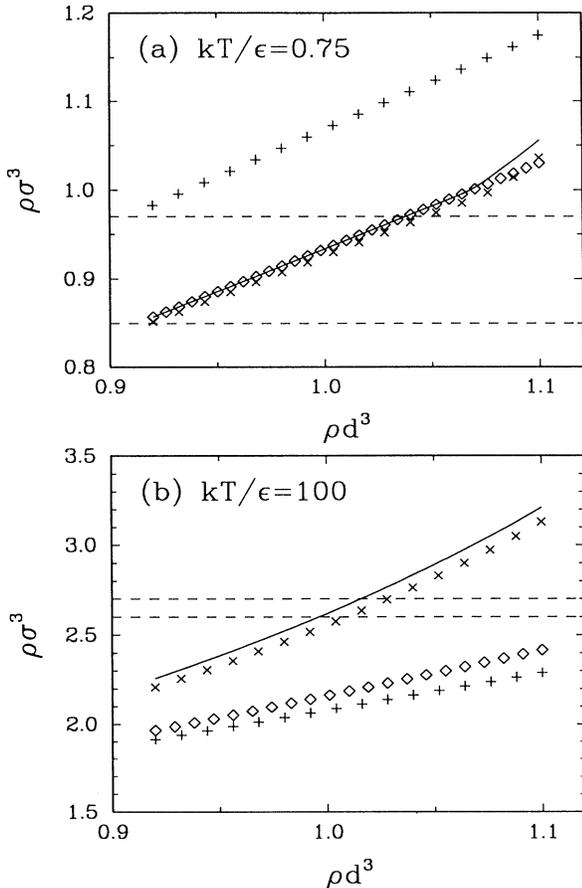
FIG. 5. Range of Lennard-Jones liquid densities that can be spanned from a hard-spheres reference state with densities $0.92 \leq \rho d^3 \leq 1.1$ at temperatures (a) $kT/\varepsilon = 0.75$ and $kT/\varepsilon = 100$. Comparison between BH (+) decomposition, WCA ($\Diamond$) decomposition, BH ($\times$), and WCA (——) approximations for the effective hard-sphere diameter for the Kang, Ree, and Ree [21] potential decomposition. The curves (— — —) correspond to the MC predictions for liquid-solid coexistence densities at these temperatures.

TABLE I. Excess Helmholtz free energy $\beta F_{ex}/N$ for the uniform Lennard-Jones liquid. Comparison between MC calculations [37,49], the predictions of Kang et al. [37], and this work using Eqs. (26) and (27) for the reference state $g(r)$. The effective hard-spheres packing fraction η predicted by [37] and this work also are compared.

| $\rho\sigma^3$ | $\beta F_{ex}/N$ | | | | η | |
	Exact	Ref. [37]	PY Eq. (26)	PY Eq. (27)	Ref. [37]	PY
			$kT/\varepsilon=0.75$			
0.7	−4.17	−4.15	−4.15	−4.15	0.393	0.394
0.8	−4.47	−4.46	−4.46	−4.46	0.448	0.450
0.84	−4.53	−4.52	−4.52	−4.52	0.470	0.472
			$kT/\varepsilon=2.74$			
1.0	1.58	1.57	1.65	1.65	0.474	0.479
1.1	2.31	2.30	2.43	2.40	0.505	0.510
			$kT/\varepsilon=5.0$			
1.0	2.20	2.13	2.19	2.20	0.435	0.439
1.279	4.26	4.19	4.37	4.29	0.512	0.518
			$kT/\varepsilon=100.0$			
1.33	2.13	2.15	2.16	2.16	0.326	0.328
1.4	2.31	2.32	2.35	2.35	0.340	0.342
2.0	4.36	4.37	4.49	4.44	0.441	0.446
2.222	5.38	5.40	5.56	5.48	0.472	0.477
2.38	6.22	6.24	6.45	6.34	0.491	0.496
2.5	6.92	6.95	7.19	7.06	0.505	0.510

both accurate to the same order [37], but the use of Eq. (26) requires additional approximations that reduce its accuracy.

IV. DESCRIPTION OF THE SOLID PHASE

A. Solid pair distribution function

Our objective is to build a DF-TP model for the LJ solid. The main requirement for the model is that it reduces to the Kang et al. [37] framework for the uniform liquid, described in Sec. III, when taken to this limit. The free energy of the reference state for the hard-sphere system is given by the GELA-DFT approximation. An issue of particular interest is the model for the solid-state pair distribution function $g_s(r)$. Analytical approximations for this function have been developed by Choi, Ree, and Ree [42], Weiss [20], and Kincaid and Weiss [43], but these expressions cannot be used in a DFT, where the objective is to generate and not use structural and thermodynamic information for the solid.

Most of the DF-TP methods developed in the past have been for inhomogeneous liquids. A variety of models have been used, ranging from a local-density approximation for $g_d(r)$ in an analysis of the gas-liquid interface [44], to the mean-field treatment of the inhomogeneous liquid confined in narrow slits [9]. Recently Tang, Scriven, and Davis [10] and Sokolowski and Fischer [45] developed a DF-TP model for inhomogeneous liquids that incorporated the effects of correlations in the liquid phase. The natural extension of this approximation to the study of uniform solids is defined by the mapping

$$g(\mathbf{r},\mathbf{r}';[\rho])\simeq g(|\mathbf{r}-\mathbf{r}'|;\hat{\rho}), \tag{28}$$

where $\hat{\rho}$ is the weighted density of the GELA approximation for the solid. The mean-field (MF) approximation corresponds to the limit $\hat{\rho}=0$ and was used by Tarazona [4].

The spherically averaged pair distribution function of the solid is written as

$$g_s(r)\equiv\frac{1}{4\pi V\rho^2}\int d\Omega\,d\mathbf{r}'\rho(\mathbf{r}')\rho(\mathbf{r}+\mathbf{r}')g(r;\hat{\rho}); \tag{29}$$

or using a manipulation proposed by Tarazona, it can be computed more efficiently as

$$g_s(r)=\frac{g_d(r;\hat{\rho})}{4\alpha rV\rho^2}\int d\mathbf{r}'\rho(\mathbf{r}')\sum_{\mathbf{R}}\frac{1}{|\mathbf{r}'-\mathbf{R}|}\{\exp[-\alpha(r-|\mathbf{r}'-\mathbf{R}|)^2]-\exp[-\alpha(r+|\mathbf{r}'-\mathbf{R}|)^2]\}. \tag{30}$$

At this point, a direct minimization of the LJ solid free energy may be performed. However, the attractive contribution to the free energy leads to superstable solid phases, and shifts the minimum in α to more structured solids than the ones found by assuming that all structural information comes directly from the hard-sphere free-energy minimization [46]. Using the mean-field approximation $\hat{\rho}=0$ yields more reasonable values for the free energy than the value of $\hat{\rho}$ from the GELA approximation. However, the mean-field model is not accurate for the uniform liquid system.

Why does the structural model of Eq. (28) fail? The solid phase $g_s(r)$ predicted from Eq. (30) with both the GELA and the mean-field approximations for $\hat{\rho}$ are compared in Fig. 6 to the pair distribution function given by Monte Carlo simulations at the same density. The functions $g_{MC}(r)/g_{MF}(r)$ and $g_{DFT}(r;\hat{\rho})/g_{MF}(r)$ are compared in Fig. 7, for the localization α at the density predicted by the GELA. Although the DF model captures the contact value (a measure of the pressure) rather accurately, it is clear from Fig. 7 that there are correlations in the solid phase that neither a mean-field model nor the DFT approximation of Eq. (28) can capture. The PY liquid pair distribution function at $\rho d^3=1.04$ also is shown in Fig. 6. For $\rho d^3\leq1.08$ Woodcock [47] found that there is a metastable hard-sphere liquid that undergoes a transition to a glass upon compression for $\rho d^3>1.08$. The PY expression for $g(r)$ loses accuracy at
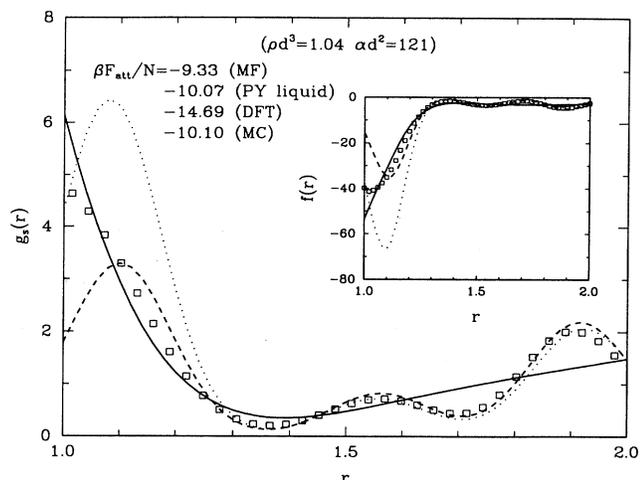
FIG. 6. Comparison of models for the hard-sphere solid pair distribution function at $\rho d^3 = 1.04$: MC results ($\square$), GELA-DFT model ($\cdot \cdot \cdot$), mean-field model ($- - -$). The solid curve corresponds to the PY liquid $g(r)$ at that density. The insert is a plot of the integrand in Eq. (17). For details see text.

those high densities, but still retains the characteristics of the MC simulations $g(r)$ for the metastable liquid.

The inset plot in Fig. 6 shows the variation of the integrand of Eq. (17) computed using Eq. (27), $4\pi r^2 \beta U_1(r) g_d(r;d)$, and plotted for the three alternative solid pair distributions at $kT/\varepsilon = 0.75$. The liquid $g(r)$ predicts perturbative contributions that are intermediate between those of the GELA and the mean-field solid pair distribution functions. The reason is that the liquid $g(r)$ lies close to the exact $g_s(r)$ within the first nearest-neighbor shell, this portion of the curve gives the most
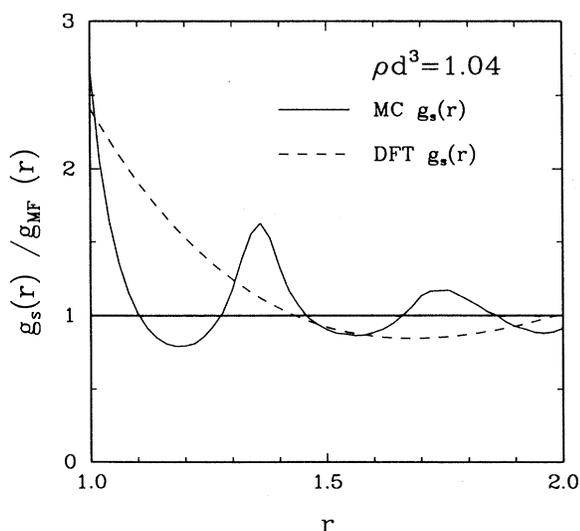
FIG. 7. Plot of $g_{MC}(r)/g_{MF}(r)$ (———) and $g_{DFT}(r)/g_{MF}(r)$ ($- - -$) for the hard spheres solid at $\rho d^3 = 1.04$, and with $\alpha d^2 = 121$.

important contributions to the free energy because the minimum of the LJ potential occurs here. Therefore, the approximation of ignoring the solid structure and using the $g(r)$ of an isotropic liquid as used by Jones and Ashcroft [48] and Curtin [13], seems reasonable and is used in our calculations for the solid.

One problem with this approximation is that the perturbative contribution is a function, rather than a functional of the density, and cannot distinguish between different crystalline structures. Therefore, the relative stability of the bcc and the fcc lattices in the LJ system cannot be explored within this approximation because any free-energy differences that arise in this model are due to the hard-sphere contributions.

B. Solid free energies

The predictions of the DF-TP model described above for the excess free energies of LJ solids with respect to an ideal gas at the same temperature and density are compared in Fig. 8 to the predictions of MC simulations reported for $0.75 \leq kT/\varepsilon \leq 100$. These predictions are compared in Table II with the results of Kang, Ree, and Ree [21], who used an analytical approximation for the hard-sphere solid pair distribution function. The packing fraction $\eta \equiv \pi/6\rho d^3$ of the effective hard-sphere liquids that correspond to the solid also are compared in Table II with the values reported by [21]. The effective hard-sphere systems resulting from the use of liquid pair distribution functions are consistently less dense than those of [21]. DF-TP results with $\eta > 0.575$ correspond to hard-sphere liquids beyond the glass transition [47] and are not very reliable.

The free-energy predictions of this approximation are

TABLE II. Excess Helmholtz free energy $\beta F_{ex}/N$ for the Lennard-Jones solid. Comparison between MC calculations [49], the predictions of Kang, Ree, and Ree [21], and this work using Eqs. (26) and (27) for the reference state $g(r)$. The effective hard-sphere packing fraction η predicted by [21] and this work also are compared. The asterisks indicate packing fractions that exceed the supercooled liquid limit.

	$\beta F_{ex}/N$				η	
		Ref.	PY		Ref.	
$\rho\sigma^3$	Exact	[21]	Eq. (26)	Eq. (27)	[21]	PY
	$kT/\varepsilon = 0.75$					
1.0	-4.48	-4.48	-4.52	-4.51	0.567	0.558
1.025	-4.41	-4.44	-4.48	-4.47	0.575	0.567
1.1	-4.17	-4.10	-4.02	-4.12	0.596	0.588*
	$kT/\varepsilon = 1.35$					
1.1	0.18	0.21	0.24	0.18	0.562	0.554
1.2	0.92	1.08	1.23	1.06	0.587	0.579*
	$kT/\varepsilon = 2.74$					
1.2	3.138	3.193	3.25	3.17	0.544	0.537
1.3	4.074	4.135	4.27	4.12	0.568	0.560
1.4	5.31	5.37	5.59	5.36	0.589	0.580*
	$kT/\varepsilon = 100.0$					
3.0		10.32	10.59	10.32	0.568	0.559
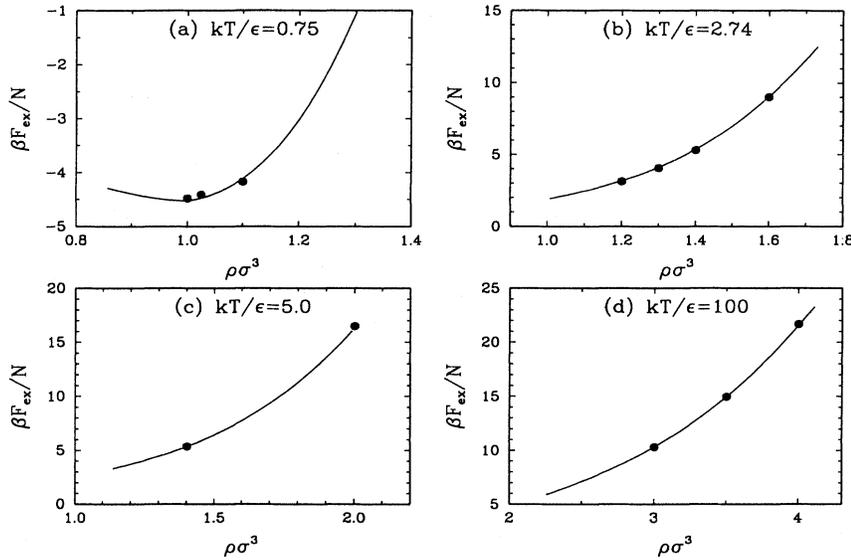
FIG. 8. Comparison of model predictions (———) of the excess free energy of LJ solids with respect to an ideal gas at the same $\rho\sigma^3$ and T, with MC simulation results from [21,49] (●) at (a) $kT/\varepsilon=0.75$, (b) $kT/\varepsilon=2.74$, (c) $kT/\varepsilon=5$, and (d) $kT/\varepsilon=100$.

reasonably accurate for all temperatures. The solid excess free energies predicted using Eq. (27) for the reference state are closer to the simulation values. Since the hard-sphere solid free energies predicted by GELA also are very accurate, this agreement is not fortuitous, but rather is a result of the TP framework used to approximate the free energy.

V. LIQUID-SOLID PHASE TRANSITION

Another test of the accuracy of the DF-TP model is the prediction of the conditions of coexistence of the LJ solid and liquid. Thermodynamic coexistence occurs when at a given temperature the two phases have equal chemical potentials and pressures:
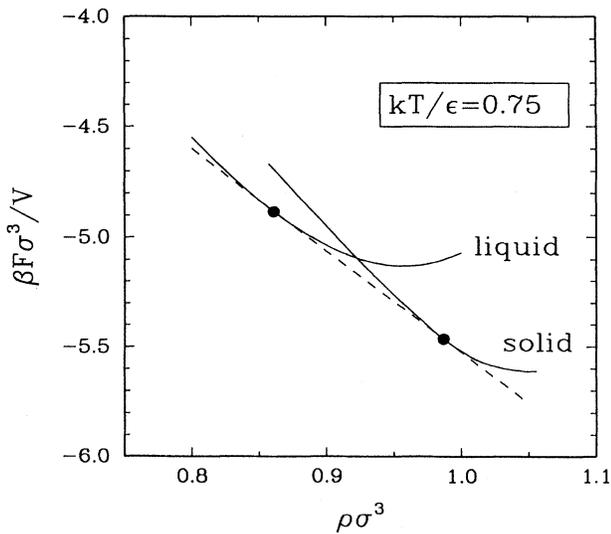
FIG. 9. Prediction of solid-liquid coexistence by double tangent construction at $kT/\varepsilon=0.75$.

TABLE III. Fluid-solid coexistence densities and pressures for the Lennard-Jones system for a range of temperatures kT/ε. Comparison between MC simulations [49,21], the predictions of Kang, Ree, and Ree [21], this work using Eqs. (26) and (27), Curtin and Ashcroft [18], and Curtin [13].

	Exact	Ref. [21]	PY Eq. (26)	PY Eq. (27)	Ref. [18]	Ref. [13]
$kT/\varepsilon=0.75$						
$\rho_s\sigma^3$	0.973	0.958	0.983	0.987	0.970	1.025
$\rho_l\sigma^3$	0.875	0.866	0.859	0.861	0.855	0.898
$P\sigma^3/\varepsilon$	0.67	0.66	0.65	0.68	0.9	2.41
$kT/\varepsilon=1.15$						
$\rho_s\sigma^3$	1.024	1.030	1.008	1.016	1.026	1.059
$\rho_l\sigma^3$	0.936	0.954	0.920	0.919	0.934	0.946
$P\sigma^3/\varepsilon$	5.68	6.41	5.44	5.39	6.4	7.62
$kT/\varepsilon=1.35$						
$\rho_s\sigma^3$	1.053	1.058	1.024	1.033	1.045	1.085
$\rho_l\sigma^3$	0.964	0.986	0.943	0.939	0.960	0.970
$P\sigma^3/\varepsilon$	9.00	9.60	8.13	7.95	9.1	10.8
$kT/\varepsilon=2.74$						
$\rho_s\sigma^3$	1.179	1.210	1.156	1.159		
$\rho_l\sigma^3$	1.113	1.144	1.093	1.092		
$P\sigma^3/\varepsilon$	32.2	36.8	31.58	30.00		
$kT/\varepsilon=5.0$						
$\rho_s\sigma^3$	1.349	1.372	1.309	1.310		
$\rho_l\sigma^3$	1.279	1.304	1.247	1.244		
$P\sigma^3/\varepsilon$	86	93	80.45	76.8		
$kT/\varepsilon=10.0$						
$\rho_s\sigma^3$	1.572	1.599	1.523	1.524		
$\rho_l\sigma^3$	1.500	1.526	1.457	1.454		
$P\sigma^3/\varepsilon$	231	247	215	205		
$kT/\varepsilon=100.0$						
$\rho_s\sigma^3$	2.706	2.750	2.614	2.613		
$\rho_l\sigma^3$	2.601	2.639	2.517	2.511		
$P\sigma^3/\varepsilon$	4800	5036	4393	4214		
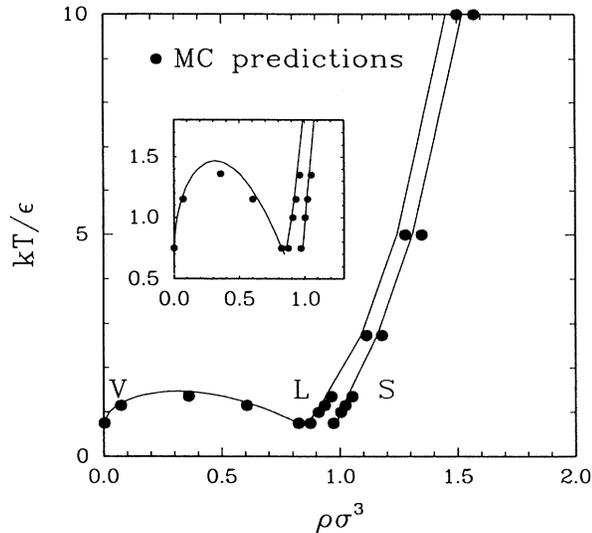
FIG. 10. Phase diagram predicted for LJ potential. The solid curves are predicted by the DF-TP analysis and the symbols correspond to MC calculations taken from [21,49].

$$\mu_s(\rho_s)=\mu_l(\rho_l) \ , \quad p_s(\rho_s)=p_l(\rho_l) \ . \tag{31}$$

The chemical potentials and pressures of both phases are easily determined from the variation of the total free energy with the density at a given temperature. The solution of Eqs. (31) corresponds to a double tangent construction, as shown in Fig. 9, for $kT/\varepsilon=0.75$. The conditions of solid-liquid coexistence are presented in Table III as predicted from the DF-TP approximations to the free energies for the solid and the liquid. The data are compared to the MC results, the predictions of Kang, Ree, and Ree [21] and the DF-TP models of Curtin and Ashcroft [18] and Curtin [13]. The predictions of the DF-TP model described here are within 5% of the values from simulations throughout the temperature range. Curtin and Ashcroft's predictions [18] are better in the low-temperature range $0.75 \leq kT/\varepsilon \leq 1.35$. However, our calculations for the free energies of both the solid and the liquid phases are more accurate, in spite of the structural corrections that are included for the solid phase in [18]. The predictions of Curtin [13], which share the same approximations for the solid phase, but use a much simpler TP scheme, are not as accurate.

The phase diagram of the LJ system for $0.75 \leq kT/\varepsilon \leq 10$ is shown in Fig. 10 as predicted from the DF-TP model. The discrepancy in the liquid-gas phase diagram is a known feature of the WCA potential decomposition scheme [33]. The agreement between our DF-TP model and the MC simulations is very good.

VI. SUMMARY

We have developed a DF-TP framework for LJ solids. The model is based on combining a nonperturbative DFT for hard-sphere systems, a Gaussian representation of the density of the solid and a thermodynamic-perturbation theory for the LJ free energies based on a reference state of a fcc hard-sphere system. Each of these approximations is tested individually by comparison to Monte Carlo simulations that exactly model the hard-sphere and LJ systems.

The predictions of solid-state structure of the nonperturbative DFT approximations for hard spheres were compared to density profiles of hard-sphere solids obtained from MC simulations. The simple model of the solid structure given by the Gaussian representation of its density is a good approximation for solids that are thermodynamically stable. The anisotropies in the density predicted by the DFT studies [28] are important only in very metastable solids and justify the application of the Gaussian approximation to the density. Monte Carlo simulations confirm that the predictions of the DFT overestimate the localization in the solid and provide additional information for the variation of the structure with density that can be used for comparison in future DFT models, where the accuracy of the structural mapping has to be reassessed.

The ability of the density parametrization to approximate the features of the inhomogeneous system is very important. Since the study of solids makes the use of flexible numerical approximations prohibitively expensive, direct comparisons with three-dimensional density profiles obtained by MC simulations is the best approach for developing more robust and realistic representations of inhomogeneous solid regions, such as the solid-melt interface, where information provided by DFT is particularly valuable.

Examination of the approximations to the spherically averaged pair distribution functions for the solid phase used in DF-TP theory revealed that the DFT and mean-field descriptions are inadequate, because both either overpredict or underpredict the attractive contributions to the free energy. Application of the pair distribution function of the supercooled liquid gave results with accuracy comparable to the free energies predicted using MC simulations to compute $g(r)$ for the reference hard-sphere solid. The most encouraging result from this effort is that the entire phase diagram of the LJ system is predicted accurately using *only* liquid-state information for a large range of temperatures.

It will be interesting to adapt the DF-TP framework with the density-dependent potential decomposition presented here to an inhomogeneous solid region, such as the melt-solid interface, where there are bulk density variations; and to explore its applicability to metallic systems, where density-dependent effective pair potentials are typically used [13].

ACKNOWLEDGMENTS

[1] R. Evans, Adv. Phys. **28**, 143 (1979).
[2] D. W. Oxtoby, Nature **347**, 725 (1990); in *Liquids, Freezing, and the Glass Transition*, edited by J. P. Hansen, D. Levesque, and J. Zinn-Justin (Elsevier, New York, 1991), and references therein.
[3] Y. Singh, Phys. Rep. **207**, 351 (1991), and references therein.
[4] P. Tarazona, Mol. Phys. **52**, 81 (1984).
[5] W. A. Curtin and N. W. Ashcroft, Phys. Rev. A **32**, 2909 (1985).
[6] A. R. Denton and N. W. Ashcroft, Phys. Rev. A **39**, 4701 (1989).
[7] J. F. Lutsko and M. Baus, Phys. Rev. A **41**, 6647 (1990).
[8] A. Kyrlidis and R. A. Brown, Phys. Rev. A **45**, 5654 (1992).
[9] T. K. Vanderlick, L. E. Scriven, and H. T. Davis, J. Chem. Phys. **90**, 2422 (1989).
[10] Z. Tang, L. E. Scriven, and H. T. Davis, J. Chem. Phys. **95**, 2659 (1991).
[11] D. M. Kroll and B. B. Laird, Phys. Rev. A **42**, 4806 (1990).
[12] J. R. Henderson, P. Tarazona, F. van Swol, and E. Velasco, J. Chem. Phys. **96**, 4633 (1992).
[13] W. A. Curtin, Phys. Rev. B **39**, 6775 (1989).
[14] X. C. Zeng and D. W. Oxtoby, Phys. Rev. A **41**, 7094 (1990).
[15] B. B. Laird and D. M. Kroll, Phys. Rev. A **42**, 4810 (1990).
[16] A. De Kuijper, W. L. Vos, J.-L. Barrat, J.-P. Hansen, and J. A. Schouten, J. Chem. Phys. **93**, 5187 (1990).
[17] A. Kyrlidis and R. A. Brown, Phys. Rev. A **44**, 8141 (1991).
[18] W. A. Curtin and N. W. Ashcroft, Phys. Rev. Lett **56**, 2775 (1986).
[19] C. Marshall, B. B. Laird, and A. D. J. Haymet, Chem. Phys. Lett. **122**, 320 (1985).
[20] J. J. Weiss, Mol. Phys. **28**, 187 (1974).
[21] H. S. Kang, T. Ree, and F. H. Ree, J. Chem. Phys. **84**, 4547 (1986).
[22] J. P. Hansen and I. R. McDonald, *Theory of Simple Liquids* (Academic, New York, 1986).
[23] P. R. Harrowell, D. W. Oxtoby, and A. D. J. Haymet, J. Chem. Phys. **83**, 6058 (1985).
[24] T. V. Ramakrishnan and M. Yussouff, Phys. Rev. B **19**, 2775 (1979).
[25] A. D. J. Haymet and D. W. Oxtoby, J. Chem. Phys. **74**, 2559 (1981).

[26] M. Baus and J. L. Colot, Mol. Phys. **55**, 653 (1985).
[27] J. L. Colot and M. Baus, Mol. Phys. **57**, 809 (1986).
[28] B. B. Laird, J. D. McCoy, and A. D. J. Haymet, J. Chem. Phys. **87**, 5449 (1987).
[29] W. G. Hoover and F. H. Ree, J. Chem. Phys. **49**, 3609 (1968).
[30] M. P. Allen and D. J. Tildesley, *Computer Simulation of Liquids* (Oxford University Press, New York, 1987).
[31] J. A. Barker and D. Henderson, Rev. Mod. Phys. **48**, 587 (1976).
[32] D. A. McQuarrie, *Statistical Mechanics* (Harper and Row, New York, 1976); R. W. Zwanzig, J. Chem. Phys. **22**, 1420 (1954).
[33] L. Verlet and J. J. Weiss, Phys. Rev. A **5**, 939 (1972).
[34] H. C. Andersen, J. D. Weeks, and D. Chandler, Phys. Rev. A **4**, 1597 (1971).
[35] J. D. Weeks, D. Chandler, and H. C. Andersen, J. Chem. Phys. **54**, 5237 (1971).
[36] F. H. Ree, J. Chem. Phys. **64**, 4601 (1976).
[37] H. S. Kang, C. S. Lee, T. Ree, and F. H. Ree, J. Chem. Phys. **82**, 414 (1985).
[38] J. H. Kim, T. Ree, and F. H. Ree, J. Chem. Phys. **91**, 3133 (1989).
[39] A. Kyrlidis and R. A. Brown, in *Computational Methods in Materials Science*, edited by J. E. Mark, M. E. Glicksman, S. P. Marsh, and P. Meakin, MRS Symposia Proceedings No. 278 (Materials Research Society, Pittsburgh, 1992).
[40] M. S. Wertheim, Phys. Rev. Lett. **10**, 321 (1963).
[41] H. L. Frisch, J. L. Katz, E. Praestgaard, and J. L. Lebowitz, J. Phys. Chem. **70**, 2016 (1966); G. A. Mansoori, J. A. Provine, and F. B. Canfield, J. Chem. Phys. **51**, 5295 (1969).
[42] Y. Choi, T. Ree, and F. H. Ree, J. Chem. Phys. **95**, 7548 (1991).
[43] J. M. Kincaid and J. J. Weiss, Mol. Phys. **34**, 931 (1977).
[44] S. Toxvaerd, J. Chem. Phys. **55**, 3116 (1971).
[45] S. Sokolowski and J. Fischer, J. Chem. Phys. **96**, 5441 (1992).
[46] A. Kyrlidis (unpublished).
[47] L. V. Woodcock, Ann. N.Y. Acad. Sci. **371**, 274 (1981).
[48] R. S. Jones and N. W. Ashcroft, J. Chem. Phys. **80**, 3328 (1984).
[49] J. P. Hansen and L. Verlet, Phys. Rev. **184**, 151 (1969).